Journal of the European Ceramic Society 20 (2000) 1483–1491

Study of the local environment around zirconium ions in polycrystalline α-alumina in relation with kinetics of grain growth and solute drag

M.K. Loudjani [a], R. Cortès [b]

[a] *Laboratoire d'Etude de Matériaux Hors d'Equilibre (LEMHE), Bat 413, 91405 Orsay Cedex, France*
[b] *Laboratoire de Physique des Liquides et Electrochimie, CNRS, UPR15, Université Pierre et Marie Curie, 75252 Paris Cedex 05, France*

Received 10 May 1999; received in revised form 7 January 2000; accepted 30 January 2000

Abstract

The aim of the present work, made up of two parts, consists in studying the behaviour of the local environment of the doping zirconium, in the polycrystalline α-alumina related to the material microstructure. At first, the kinetics of grain growth has been studied, and local chemical analyses on thin foils at grain boundaries using the energy dispersive X-ray spectroscopy (EDXS) technique, were performed. In the second part, we shall consider the evolution of the local order around the doping element, related to the microstucture, by X-ray absorption spectroscopy (XAS) measurements. This study was performed on doped α-polycrystalline alumina (0.03 wt% ZrO_2) samples. According to the experimental results, we can show a great interaction between the zirconium and the grain boundaries of the alumina: during the grain growth, grain boundaries drag most of the doping element in solid solution. A transition in the environmental configuration around the doping in grain boundaries is observed, when the segregation ratio of the zirconium in grain boundaries reaches the value of about $(4\pm2)\times10^3$. In these conditions, a change in the local order is observed, around the segregated zirconium. This change varies from a statistical disorder to an ordered state, and can be described as an assembly of nanocrystalline metastable, tetragonal zirconia particles. This transition of the environmental configuration in grain boundaries is correlated to the increase of the grain growth velocity, according to the kinetics studies.

Keywords: Al_2O_3; Grain growth; Segregation; X-ray methods; ZrO_2

1. Introduction:

Alumina is a stoichiometric oxide, so its transport properties and its microstructure are controlled by extrinsic defects or doping element contents.

Because of the great size and the charge effects, these doping elements or impurities mostly segregate along grain boundaries of the alumina. At low temperatures, kinetics of equilibrium segregation is often neglected if we take into account the small anionic and cationic diffusion coefficient values in this oxide.[1,2] When high temperatures are reached, boundaries may be moving; consequently, kinetics of enrichment of boundaries in doping elements depends on the dragging effects of the solute or doping: the grain growth causes the dragging of the solute because of the moving boundaries, and a great enrichment of the grain boundaries in doping elements consequently occurs.[3–6] That can be observed during the sintering of doped alumina powder.[7,8] In the same way, nucleation and growth of the native alumina scales expanded upon alloys alumina-formers, containing impurities such as yttrium, zirconium can be considered as discussed previously.

This segregation of impurities substantially affects the physical and chemical properties of the material grain boundaries. For a few years, the segregation studies, frequently mentioned in literature, were conducted using chemical analysis techniques with an electron beam, such as Auger electron spectroscopy for examining surface segregation. These studies were also performed using energy dispersive X-ray spectroscopy or electron energy loss spectroscopy (EELS) for analysis on thin foils, in the case of investigations of the interfaces.[9–15] Whereas these techniques consist, in most cases, in a local analysis (because of the small size of the electron beam), the information related to the analysed zone at the interfaces prevents the obtaining of the true atomic arrangement close to the doping elements which segregate into those interfaces.[15–17]

0955-2219/00/$ - see front matter
PII: S0955-2219(00)00035-2

In relation to the kinetics of the grain growth, the variation of the true local environment of the doping zirconium segregated along grain boundaries has been studied by X-ray absorption spectroscopy technique (XAS) combined with the microscopy and local chemical analysis on thin foils. Indeed, because of its high sensibility, and thanks to a larger analysed bulk of grain boundaries ($\approx 10^9$ grains boundaries in the case of XAS studies), when compared to the EDXS analyses on thin foils, and since the microstructure was controlled, the XAS method was well adapted to the determination of the local order around the doping (zirconium) in the α-alumina in relation to its microstructure. It was also possible to evaluate the threshold of the zirconium concentration in grain boundaries from which the "disorder–order" transition can occur. The aim of this study consists in clarifying the relation between the transition of the environmental configuration around the zirconium in grain boundaries and the kinetics of grain growth.

2. Materials and experimental procedure

2.1. Materials

The studies were performed on zirconium-doped α-polycrystalline alumina samples ($C_0 = 0.03$ wt% ZrO_2) obtained by hot pressing at 1400°C for 15 min under a low oxygen partial pressure ($pO_2 \approx 10^{-13}$ atm).[1] The α-alumina powder was provided by "Baikowski, France".[15,17] The average grain size of the sintered materials was $\overline{G} \approx 0.57 \pm 0.3$ μm. In this final stage of the sintered material, the zirconium is in a solid solution; this local structure around zirconium had been previously determined.[15,17]

The sintered samples were first polished and annealed at 1400°C in air for times varying from 1 to 501.5 h at 1400°C. To improve grain boundary grooving, in the case of low annealing time ($t \leqslant 1$ h), the surface of the samples were chemically treated in a solution of sodium tetraborate ($Na_2B_4O_7$) and thermally etched at 1000°C for 2 h. The microstructure of all samples was observed on a digitised scanning electron microscopy (SEM) and average grain size obtained by images analysis. Annealing times for heat treatment and grain size of doped α-alumina samples are reported on Table 1.

2.2. XAS experiment

The XAS studies, at the K-edge of zirconium, were performed on five α-polycrystalline alumina samples (Zr1–Zr5), doped with the same content of zirconia ($C_0 \approx 300$ wt ppm ZrO_2). The results are correlated to the kinetics studies of grain growth obtained on the same alumina samples.

A tetragonal single crystal of yttrium doped-zirconia ($ZrO_2 + 3$ mol% Y_2O_3) was used as standard for the XAS study.[15–17] The experimental XAS measurements (in transmission and fluorescence modes) were performed at low temperature (12 K) at LURE-DCI (Orsay), using the EXAFS-II spectrometer.[25] The energies were calibrated by assigning the maximum inflection point of the zirconium K-edge in tetragonal ZrO_2 to17997 eV.

On account of the low concentration of the doping element, the measurements on doped-alumina samples were conducted on the fluorescence mode, when the tetragonal zirconia was studied in transmission mode.

Table 1
Annealing times of the heat treatment and grain size of doped α-alumina samples

Samples	Annealing temperature (°C)	Annealing time (h)	Mean grain size (μm)
Zr1	1400	1	0.57±0.3
Zr2	1400	24	0.97±0.39
Zr2′	1400	72	1.25±0.63
Zr3	1400	144	2.76±1.56
Zr4	1400	216	2.83±1.58
Zr5	1400	501.5	2.96±1.44

3. Analysis results

3.1. Microstructure and image analysis (Fig. 1a, b)

The α-alumina samples show a population with a homogeneous grain size (without abnormal grain growth). For each sample, an assembly of about 750 grains was needed to obtain reliable distributions and estimate the grain size (Fig. 2a, b). The average grain size varies from $\overline{G} = 0.57 \pm 0.3$ μm (sample Zr1) to 2.96±1.4 μm (sample Zr5).

3.2. Kinetics grain growth results and discussion

The curve showing the growth kinetics was established from the granulometric distribution (Table 1). The grain growth laws performed as a function of time during heat treatment are reported on Figs. 3 and 4. Two variation areas can be observed: for $t \leqslant 72$ h and for $t \leqslant 144$ h: the grain growth law is given by (Fig. 3a, b):

$$G^m - G_0^m = kt \quad (1)$$

where G represents the average grain size (μm) at time t (in h), G_0 the initial average size, k is a kinetic constant, and m is an integer whose value depends on the diffusion

[1] Zirconium-doped α-polycrystalline alumina was obtained by hot pressing by P. Carry: LPTCM-UMR 564-CNRS, INPG-UJF/ENSEG Domaine universitaire 38042 St. Martin d'Hères cedex France.

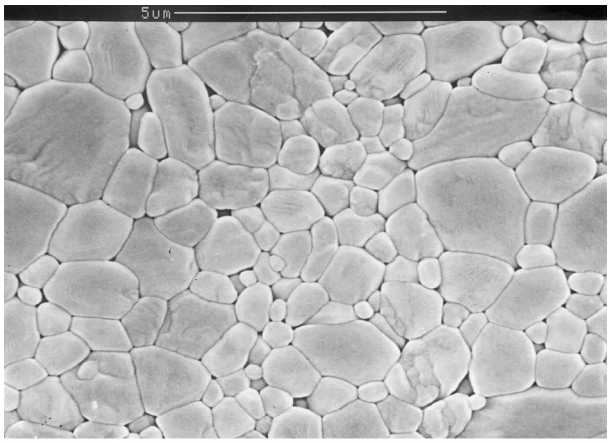

(a)

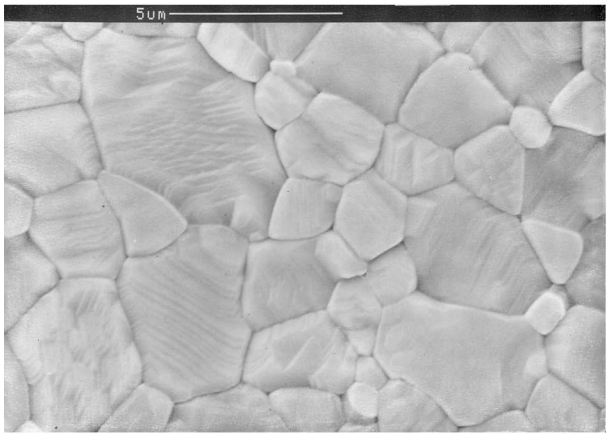

(b)

Fig. 1. Microstructure concerning the two polycrystallyne doped alumina samples. (a) Zr1 and (b) Zr5.

mechanism which is responsible for grain growth.[3–5,18–22] The regression straight lines are best adjusted to a value of m varied between 3 and 4. The best fit obtained for grain growth law and the corresponding grain growth rate, using linear regression, are reported in Table 2.

These equations represent the interaction between the grains boundaries movement and the moving impurities. The presence of a restraining force, on moving grain boundary, opposite to the grain growth driving force, due to the doping drag, explains why the velocity decreases. Then the velocity of grain growth may be seen as inversely proportional to solute concentration in grain boundaries.

After a heat treatment of 72 h, a discontinuous step rises in growth law when the mean grain size reaches a value of about $\overline{G}\approx 1.25\pm 0.6$ μm. Then the velocity of the grain growth reaches a maximum (Fig. 3b).

When a boundary is moving, the solute grain boundary concentration increases. The zirconium diffuses along the grain boundaries, to form particles of zirconia. These nanocrystalline second phase particles exert a strong pinning on grain boundaries, the pinning pressure being determined primarily by the volume fraction/interface, the distribution and size of the particles. When particles coalesce (principally in triple junctions), the number of particles intersecting the unit area of the boundary decreases and they become motionless, so that the boundary can break away; in this case, it can be observed a jump on the kinetics grain growth curves.

In the case of grain size growth controlled by coarsening particles,[3–5,18–22] the rate of growth is controlled by the rate of change particle size. Then the rate of particle coarsening will depend on the rate controlling mechanism. If the particle growth is controlled by bulk diffusion (D_b), then:

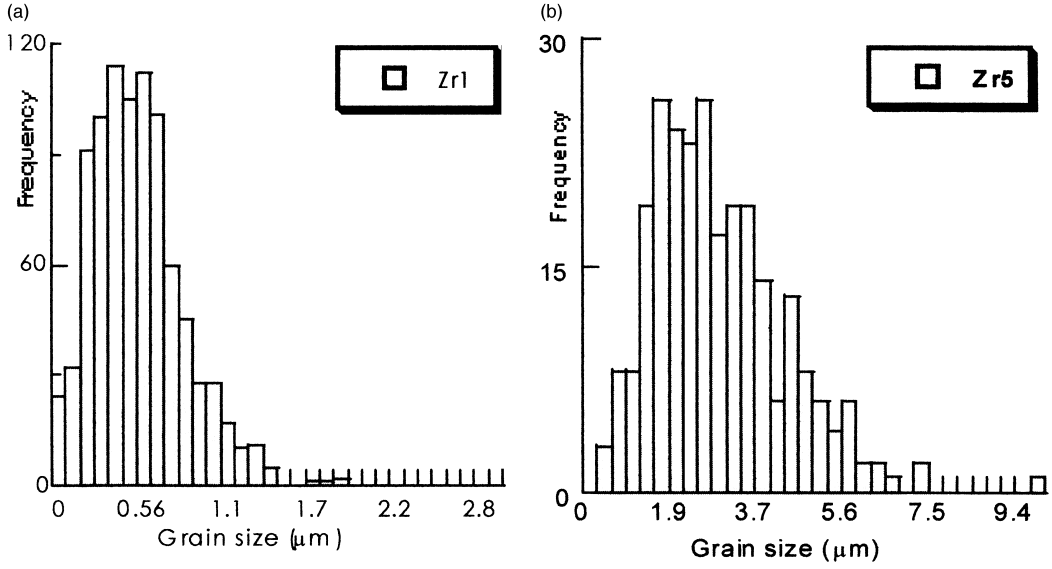

Fig. 2. Grain size distribution for (a) Zr1 and Zr5 samples.

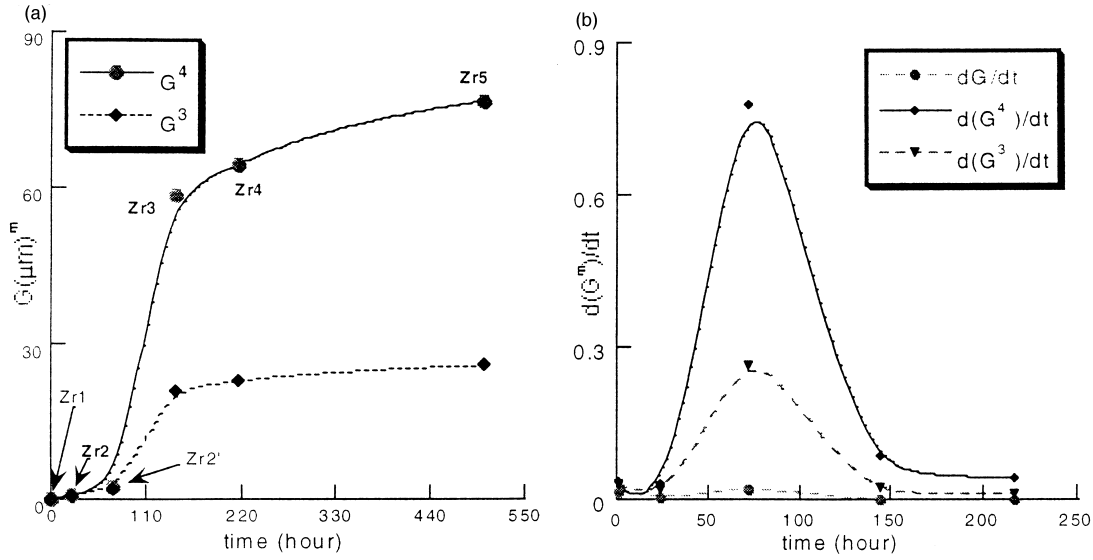

Fig. 3. (a) Grain growth kinetics and (b) grain-growth rates for alumina-samples (Zr1–5).

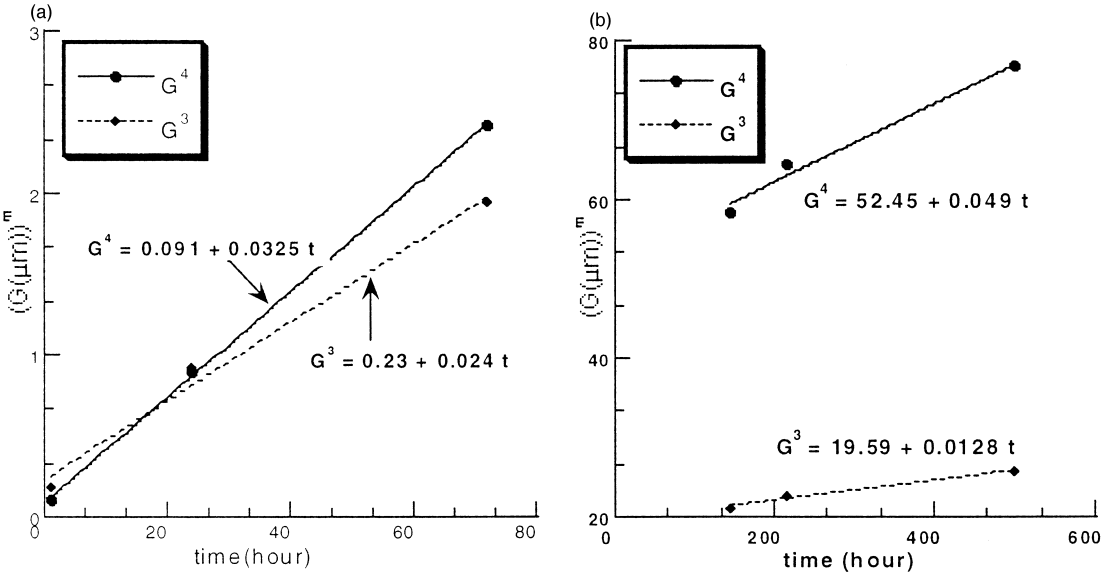

Fig. 4. Grain-growth kinetics laws for different time ranges: (a) $t < 72$ hours and (b) for $t > 144$ hours.

$$G^3 - G_0^3 = c_1 D_b t \quad (2)$$

whereas for particle growth controlled by diffusion along the interfaces (D_{gb}), it is written:

$$G^4 - G_0^4 = c_2 D_{gb} t \quad (3)$$

3.3. Results of the local chemical analysis on thin foils and discussion

The EXDS analyses were only performed on sample grain sizes which were the smallest (Zr1) and the largest (Zr5). Because of the high dilution and in view of the minimal quantity (C_{MD}) required in EXDS to be determined (in case of our samples, $C_{MD} \approx 0.08$–0.09wt% ZrO_2),[23] zirconium was not detected in Zr1 thin foils. In case of Zr5 sample, zirconium was mainly detected at triple junctions of the material.

The analysis results obtained from 20 triple junctions show that the apparent concentrations ($C_{gb.ap.}$ in ZrO_2) vary as $0.11\% \leqslant C_{gb.ap} \leqslant 0.4$ wt%. If we consider the apparent concentration measurements at grain boundaries, the true grain boundaries "$C_{gb.R} \gg$ and bulk "$C_{b.R}$" concentrations can be given[15–17] by resolving parametric Eqs. (4) and (5):

$$f_1 C_{gb.R} + (1 - f_1) C_{bR} = C_{gb.ap.} \quad (4)$$

$$f_2 C_{gb.R+}(1 - f_2) C_{bR} = C_0 = 0.03\text{wt\%}ZrO_2 \quad (5)$$

Table 2
Kinetics law of grain and velocity growth

Time (in h)	$t \leqslant 72$	$t \leqslant 144$
Grain-growth kinetics $G^m = kt - G_0^m (m = 4)$	$G^4 = 0.0325t + 0.091$	$G^4 = 0.049t + 52.447$
Grain-growth rate $V = \frac{dG}{dt}$ (μm/h)	$\frac{0.008125}{(0.091 + 0.0325t)^{3/4}}$	$\frac{0.01225}{(52.447 + 0.049t)^{3/4}}$
Grain-growth kinetics $G^m = kt - G_0^m (m = 3)$	$G^3 = 0.0234 + 0.024t$	$G^3 = 19.59 + 0.01283t$
Grain-growth rate $V = \frac{dG}{dt}$ (μm/h)	$\frac{0.008}{(0.0234 + 0.024t)^{2/3}}$	$\frac{0.00427}{(19.59 + 0.01283t)^{2/3}}$

Where f_1 represents the grain boundary volume fraction related to the analysed volume at triple junctions ($f_1 \approx \frac{6\delta}{\pi D}$, where $\delta \approx 0.5$ mm is the average width of the grain boundary, $D \cong 160 \pm 10$ nm the average diameter of the electron beam) and f_2 represents the volumic ratio of the grain boundaries in the polycrystalline sample, with a mean grain size $\bar{G}(f_2 \approx \frac{3\delta}{\bar{G}})$. The results of this analysis, taking into account the areas of variation of the parameters C_0, $\bar{G}$, $C_{gb.ap.}$ and D such as: $C_0 = 300 \pm 50$ wt ppm ZrO_2, $\overline{G} = 2.96 \pm 1.44$ μm, $0.0003\% \leqslant C_{gb.ap.} \leqslant 0.3\%$, $D = 160 \pm 10$ nm, reveal an average enrichment at grain boundaries ($\overline{S} = \bar{S} = \frac{C_{gbR}}{C_{bR}}$) which is about $2.10^3 \leqslant \overline{S} \leqslant 6.10^3$.

The kinetic enrichment of grain boundary in zirconium cannot be predicted from the segregation equilibrium model this fact has been suggested by McLean.[24] In such a model, the time dependence of the grain boundary in two semi-infinite half crystals, is given by:

$$\frac{C_{gb}(t) - C_{gb}(0)}{C_{gb}(\infty) - C_{gb}(0)} = 1 - \exp\left(\frac{4D_b t}{\alpha^2 \delta^2}\right) \operatorname{erfc}\left(\frac{2\sqrt{D_b t}}{\delta \alpha}\right) \qquad (6)$$

$\alpha = \frac{C_{gb}(\infty)}{C_0}$ is the saturation ratio of the boundary, C_0 represents the bulk concentration and $C_{gb}(t)$ the grain boundary concentration of the doping at time t, δ being the average size of the boundary, and D_b the bulk diffusivity coefficient. The experimental diffusion coefficient value of zirconium in α-alumina at 1400°C, determined in our present study is $D_b \approx 4.2 \mathring{A}^2 s^{-1}$.

From Eq. (6), we can estimate the time needed to build-up enrichment not far from saturation. When the left hand side of Eq. (6) is equal to 85%, the value:

$\frac{2\sqrt{D_b t}}{\delta \alpha}$ is about 3.55, then the time required to have an enrichment close to our experimental values:

$\overline{S} = \alpha = \frac{C_{gbR}}{C_{bR}} \approx 2.10^3$, is about 2.4 years. This time is not convenient with our experimental results.

However, if it is assumed that a moving boundary, with an average velocity V_{gb}, drags most of the zirconium in solid solution, then the enrichment of the boundary can be expressed as:

$$C_{gb}(t) = C_0 + \int_0^{72} \frac{C_0 V_{gb} A}{A\delta} dt + \int_{144}^{501.5} \frac{C_0 V'_{gb} A}{A\delta} dt \qquad (7)$$

Where A is the average grain surface, C_0 the average concentration in the starting material, and V_{gb} (μm/h) the average boundaries velocity, experimentally defined when times are $t \leqslant 72$ h or $144 \leqslant t \leqslant 501.5$ h. The mean enrichment ratio, when taking the grain growth laws ($G^m - G_0^m = kt$, with $m = 3$ or 4) reported on Table 2, is about: $1769 \leqslant \frac{C_{gb}}{C_0} \leqslant 2209$. These values are in good agreement when compared to those obtained from experiments chemical analysis on thin foils.

3.4. XAS results and discussion

The X-ray absorption spectra were analysed using standard procedure.[25–31] Fig. 5a,b shows spectra $\chi(k)$ of samples (Zri, $i = 1$–5 and ZrO_2). It can be seen that the EXAFS spectra obtained for Zr4–Zr5 samples and tetragonal zirconia are homothetic especially for the largest values of wave vector k (Fig. 5a).

Figs. 6a–e, show, for α-alumina samples (Zr1–5) doped and for standard sample, the Fourier transform magnitude spectrum (uncorrected for phase shift). We can observe the evolution of the environmental configuration around zirconium.

The Fourier transform (FT) of EXAFS spectra as shown in Figs. 6a–e, were carried out within the same scale in k space from 3.2 to 14.2 $Å^{-1}$ and with an identical width of Kaiser window [29].

The $F(r)$ curves show peaks that correspond to the neighbouring j shells. In such a representation, these peaks are situated at distances smaller than the true R_j interatomic distances since the total phase shift $\phi j(k)$[26] is not considered. The Fourier transform (FT) peaks for Zr–O shell and Zr–Zr shell were isolated and the signals were back-transformed into k space. A non-linear

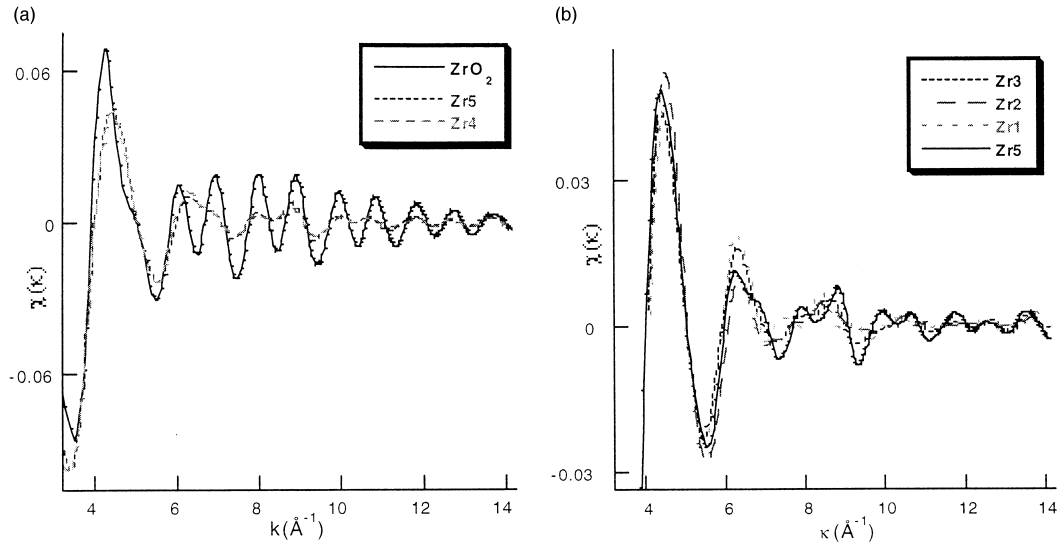

Fig. 5. Normalised oscilatory part of the absorption spectra of standard oxides (tetragonal zirconia) and polycrystalline doped-alumina samples determinated at 12 K; (a) is relative to samples with largest grain size (Zr4–Zr5) and (b) for smallest grains size (Z1–3).

least-squares fitting procedure was applied to obtain the local structure parameters, by taking into accounts the phase shift.[25–29]

For standard and α-alumina doped samples the distances R_j between the central atom and its neighbouring ions and the neighbouring number N_j were calculated and are mentioned in Table 3.

The first peaks (*A*) at about 1.6 Å in FT spectra (Fig. 6a–e) correspond to the nearest oxygen neighbours around zirconium (Zr–O) shell. It can be seen that the integrated area under each peak increases when the grains grow but remains lower than the peak of the standard sample.

The second peak (*B*) at about 3.2 Å originate from the contribution of Zr–Zr atomic pairs. The coordination number of the Zr–Zr shells for Zr4–5 samples is more important than for Zr3 sample, so that a second peak on Zr1–Zr2 samples is not observed. With a decrease of grain growth, the amplitude of the second peak decreases. This implies the breakdown of the long-range order in the structure.

3.4.1. Discussion about the local structure around the zirconium in case of Zr3–Zr4–Zr5 sample

The $F(r)$ curve shows two peaks (Fig. 6c–e):

The first peak (*A*) represents an oxygen shell (<Zr–O>), located at a mean distances of: $R_j = 2.09 \pm 0.06$ Å, $R_j = 2.10 \pm 0.06$ Å and 2.096 ± 0.06 Å respectively. These first neighbours are located at a distance from the central atom, which is similar to that observed on the tetragonal ZrO_2 sample. A difference appears on the total number of oxygen neighbours (Table 3).

Concerning the fit of the second peak (*B*): the shell distributions of Zr atoms around the zirconium absorber atom in this sample are similar to those of the metastable tetragonal zirconia–ZrO_2 compound. A significant shell is made of zirconium ions (<Zr–Zr>), the average distance from the central atom of which is comparable to those in the tetragonal ZrO_2. The contribution of oxygen neighbours on the amplitude of the *B*-peak is very small. Though the distances are very similar to that in the tetragonal ZrO_2 phase, the number of zirconium neighbours is less half lower than that in the tetragonal zirconia. This small coordination number observed on <Zr–Zr> shell is due to the small size of zirconia particles.[15–17,32,33]

From the EDXS results, it may be considered that the zirconium detected on this sample by XAS analysis is the zirconium, which appears mainly, located along grain-boundaries and triple junctions. Then zirconium, in this samples, forms little nanometric clusters of a tetragonal zirconia. The zirconium ions located at the surface of these clusters may predominately contribute to the XAS signal. With such an assumption, justified by the statistic disorder, the distances between the Zr ions become undefined; that is why the coordination number in the Zr–Zr shell decreases.

The amplitude of this peak increases with the grain growth. Then the observation of the second neighbours of zirconium shell is correlated to the increase in velocity observed on grain growth laws (Fig. 3).

3.4.2. Discussion about the local structure around the zirconium in case of Zr1–Zr2 samples (Fig. 6a, b)

The $F(r)$ curve shows only one important peak: the peak (*A*) corresponds to the oxygen ion shell that includes the first neighbours of the zirconium absorber atom in the samples. An oxygen shell is used to fit the peak containing about $N_j \approx 3.8 \pm 0.7$ oxygen ions and located at a mean distances of $R_{(Zr-O)} \approx 2.13 \pm 0.05$ Å and 2.10 ± 0.05 Å respectively for Zr1 and Zr2.

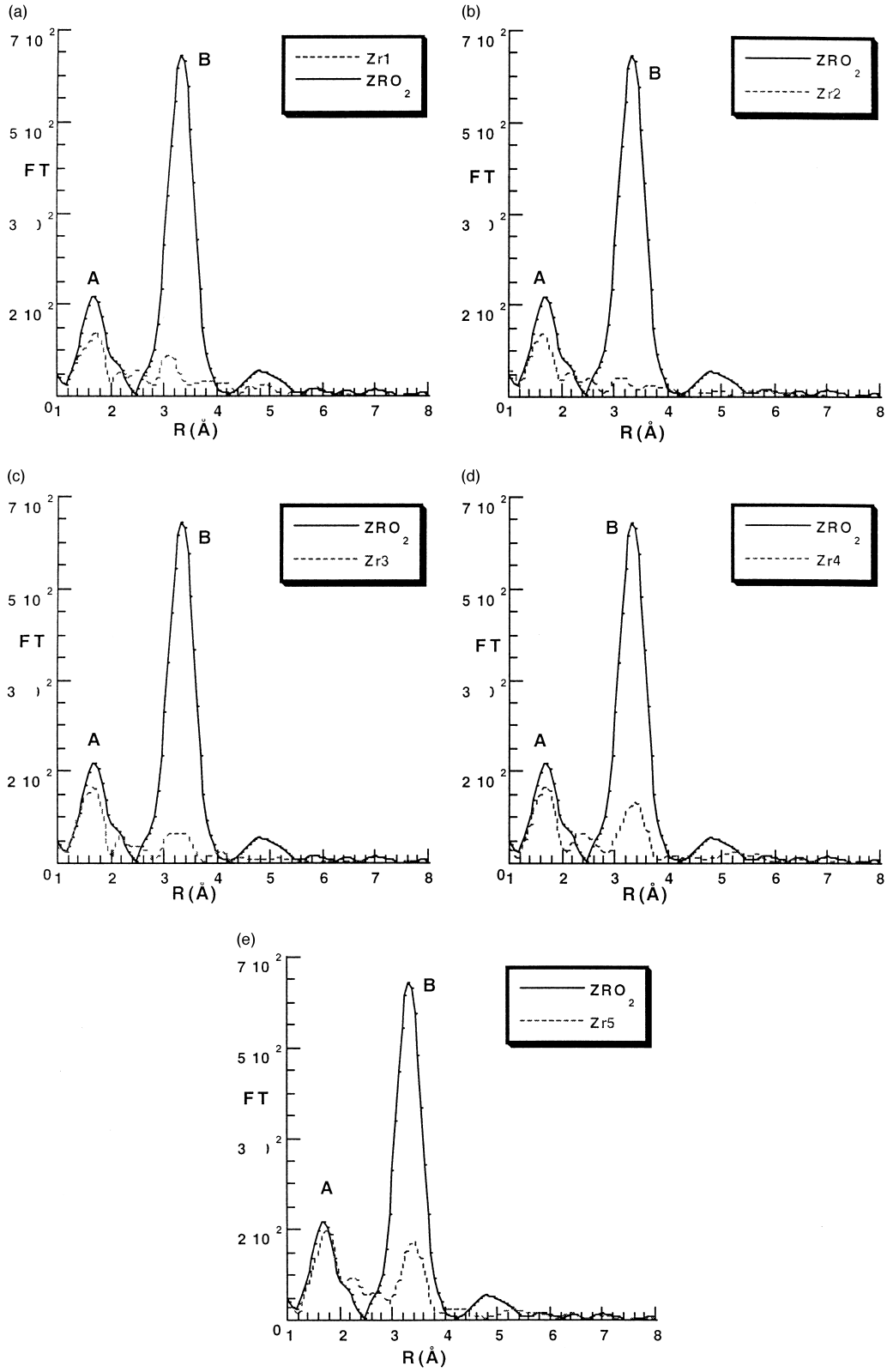

Fig. 6. Fourier-transform magnitude spectrum (uncorrected for the phase shift) of tetragonal zirconia and polycrystalline doped-alumina samples: (a)Zr1, (b) Zr2, (c) Zr3, (d) ZR4, (e) Zr5 determinated at 12 K in relation with grain size.

Table 3
Distances R_j (Å) and neighbours N_j determined for the doped α-alumina and tetragonal zirconia at 12 k

Samples	Shell (Zr–O) Peak A		Shell (Zr–Zr) Peak B	
	R_J(Å)±0.02	N_J±0.7	R_J (Å)±0.02	N_J±0.7
Zr1	2.127	3.8	No peak	≈0
Zr2	2.104	3.8	No peak	≈0
Zr3	2.09	5	3.50	0.5
Zr4	2.10	5.3	3.634	1.6
Zr5	2.096	6	3.66	1.7
ZrO_2	2.09	4	3.575	4
	2.30	4	3.657	8

The absence of a significant peak corresponding to the second neighbours in zirconium shell suggests that zirconium ions are either in a solid solution on aluminium site ($|Zr_{Al}|^{\bullet}$)[34] or in grain-boundaries as an unordered phase.

The mean equilibrium distance between zirconium and first neighbours oxygen shell ($< Zr_{Al} - O >_{Al_2O_3} \approx 2.1\mathring{A}$), determined on samples Zr1–Zr2, are more important that the smallest mean equilibrium distance aluminium-oxygen ($< Al - O >_{Al_2O_3} \approx 1.91\mathring{A}$) in non doped α-alumina.[30,31] This is mainly due to the difference between the ionic radius of zirconium and aluminium in octaedric site ($R_{Zr^{4+}} \approx 0.8\mathring{A}$, $R_{Al^{3+}} \approx 0.54\mathring{A}$).

Then the local lattice distortion around the zirconium induces an elastic strain of: $\varepsilon \approx \frac{R_{<Zr-O>Al_2O_3} - R_{<Al-O>Al_2O_3}}{R_{<Al-O>Al_2O_3}} = \frac{2.1-1.91}{1.91} \approx 10\%$, which generates an important local stress of the order of: $\sigma = E\varepsilon = 40$ Gpa, E is the Young modulus of α-alumina ($E \approx 400$ Gpa). This value of the stress is comparable to the shear stress at low temperature in α-alumina [35]. This important elastic strain can be explained if we assume a local modification of the structure such as the introduction of defect structure around the doping element. According to the defect formation equation in α-alumina we can write:

$$ZrO_2 \Longleftrightarrow Zr^{\bullet}_{Al} + 5/7V'''_{Al} + 4/7V^{\bullet\bullet}_{O} + 2O^{x}_{O}$$

If the zirconium is surrounded by this complex defect either in the bulk or in the grain boundaries a local disorder around zirconium can exist and explain the decrease of the coordination number around the doping element in the first oxygen shell ($N_j \approx 3.8$ instead of $N_j = 6$).

4. Conclusion

This study shows an important interaction between moving grain boundaries, and doping zirconium. Grain boundaries are shown to drag zirconium in polycrystalline α-alumina when they migrate. The dragging phenomena of the doping by grain boundaries regulates the kinetics during the grain growth: $G^m - G_0^m = kt, m = 3-4$. The transport mechanism, which controls the grain growth, described as a law $G^4 - G_0^4 = kt$ is mainly made of diffusion along grain boundaries.

The segregation rate in alumina grain boundaries is governed by the kinetics of the dragging phenomena of the doping when grain boundaries are migrating. The saturation rate of the α-alumina grain boundaries in a solute element, at 1400°C, is obtained for a mean grain size of about 1.25 μm and estimated to $S_{gb} \approx (4 \pm 2) \times 10^3$. The grain growth mechanism is a function of the time: at first, the moving of the boundaries is restrained because of the dragging of the doping when grain boundaries are migrating. Secondly, when the saturation rate in doping element of grain boundaries is reached, the grain growth mechanism is controlled in the grain boundaries, by the nucleation and the coarsening kinetic, of the zirconia oxide particles. The coarsening of the zirconia oxide particles is the origin of the step rise in the kinetic curves of the grain growth and explains the increase of the boundary velocity.

The XAS study at the K-edge of zirconium in doped α-alumina allows pointing out the true local structure around zirconium in grain boundaries. So, in the case of a controlled microstructure, using the XAS technique, the real local environment of the doping in grain boundaries, and the threshold of the doping concentration from which the "disorder–order" transition can occur, have been determined.

In solid solution, in grain boundary or in the bulk, the zirconium is surrounded by a complex defect.

Acknowledgements

The authors are grateful to Professor P. Carry (LPTCM-UMR 564- CNRS, INPG- UJF/ENSEG Domaine universitaire 38042 St. Martin d'Hères cedex France) for providing zirconium-doped α-polycrystalline alumina.

References

1. Le Gall, M., Lesage, B. and Bernardini, J., Self diffusion in α-Al2O3. I. Aluminium single crystal. *Phil. Mag. A*, 1994, **70**, 761–773.
2. Moya, E. G., Lesage, B., Loudjani, M. K. and Grattepin, C., Yttrium diffusion in α-alumina single crystal. *J. Eur. Ceram. Soc.*, 1998, **18**, 591.
3. Ashby, M. F. and Centamore, R. M. A., The dragging of small oxide particules by migrating grain boundaries in copper. *Acta Met.*, 1968, **16**, 1081–1092.
4. Brook, R.J., *Treatise on Materials Science and Technology, Vol. 9, Ceramic Fabrication Processes*, ed. Franklin F. Y. Wang. Academic, 1976, pp. 331–363.

5. Brook, R. J., The impuity-drag effects and grain growth kinetics. *Scripta. Metal*., 1968, **2**, 375–378.
6. Cahn, J. W., The impurity-drag effect in grain boundary motion. *Acta Met*., 1962, **10**, 789–798.
7. Gruffel, D. and Carry, C., Effect of grain size on yttrium grain boundary segregation in fine-grained alumina. *J. Eur. Ceram. Soc*., 1993, **11**, 189–199.
8. Sato, E. and Carry, C., Yttrium doping and sintering of submicrometer-grained α-alumina. *J. Am. Ceram. Soc*., 1996, **79**, 2156–2160.
9. Nanni, P., Stoddart, C. T. H. and Hondros, E. D., Grain boundary segregation and sintering in alumina. *Mat. Chem*., 1976, **1**, 297–320.
10. Johnson, W. C., Grain boundary segregation in ceramics. *Metall. Trans. A*, 1977, **9**, 1413–1422.
11. Kingery, W. D., Segregation phenomena at surface and at grain boundaries in oxides and carbrides. *Solid State ionics*, 1984, **12**, 1–9.
12. Bender, B., Williams, D. B. and Notis, R., Investigation of grain-boundary segregation in ceramic oxides by analytical scanning transmission electron microscopy. *J. Am. Ceram. Soc*., 1980, **63**(9), 542–546.
13. Bouchet, D., Dupau, F. and Lartigue-Korinek, S., Structure and chemistry of grain boundaries in yttria doped aluminas. *Micro. Microanal. Microstruct*., 1993, **4**, 561–573.
14. Mackrodt, W. C. and Tasker, P. W., Segregation isotherms at the surfaces of oxides. *J. Am. Ceram. Soc*., 1989, **72**(9), 1576–1583.
15. Loudjani, M. K., Cortès, R. and Carry, P., Etude de l'environnement et de la chimie locale autour du dopant zirconium dans l'alumine-α en relation avec la microstructure. *J. de Phys*., 1999, **IV**(9), Pr4–135.
16. Loudjani, M.K., Cortès, R. in *Proceedings of the 9th International Conference on X-ray Absorption Fine Structure ESRF-Grenoble, J. Phys. IV France 7, Colloque C2*. Suplément au journal de physique III d'avril 1997 ed. C. Brown, EDP Sciences, Les Ulis 1997, p. 1209–1211.
17. Loudjani, M. K. and Cortès, R., Study of local structure around zirconium ions in grain boundaries of polycrystalline α-alumina by X-ray absorption spectroscopy and chemical analysis of thin foils. *J. Eur. Ceram. Soc*., 1999, **19**, 2659–2666.
18. Hillert, M., On the theory of normal and abnormal grain growth. *Acta Metall*., 1965, **13**, 227–238.
19. Ardell, A. J., On the coarsening of grain boundary precipitates. *Acta Metall*., 1972, **20**, 601–609.
20. Humphreys, F. J. and Haterly, M., *Recrystallistion and Related Annealing Phenomena*. Pergamon, Oxford, 1996 p. 280.
21. Gottstein, G. and Shvindlerman, L. S., Theory of grain boundary motion in the presence of mobile particles. *Acta Metall. Mater*., 1993, **41**(11), 3267–3275.
22. Jianxin Fang, A., Thompson, M., Harmer, M. P. and Cahn, H. M., Effect of yttrium and lanthanium on the final-stage sintering behavior of ultrahigh-purity alumina. *J. Am. Ceram. Soc*., 1997, **80**(8), 2005–2012.
23. Pozsgai, I., *Trace Element Analysis in the SEM. European Microscopy and Analysis*, November 1993, pp. 31–33.
24. McLean, D., *Grain Boundaries in Metals*. Clarendon press, Oxford, 1957 pp. 124–143.
25. Goulon, J., Lemonier, M., Cortès, R., Retournard, A. and Raoux, D., Developement of new energy scanning (4-30 keV) EXAFS-II spectrometer at LURE. *Nuclear Instrument and Methods*, 1983, **208**, 625.
26. Sayers, D. E., Lytle, E. W. and Stern, E. A., New technique for investigation noncrystalline structures: Fourier analysis of the extended X-ray-absorption fine structure. *Phys. Rev. Let*., 1971, **27**(18), 1204–1207.
27. Teo, B. K. and Lee, P. A., Ab Inition calculations of amplitude and phase functions for extended X-ray absorption fine structure spectroscopy. *J. Am. Chem. Soc*., 1979, **101**, 2815–2831.
28. McKale, A. G., Knap, G. S. and Chan, S. K., Practical Method for full curved-wave theory analysis of experimental extended X-ray-absorption fine structure. *Phys. Rev. B*, 1986, **33**, 841.
29. Bonnin, D., Kaiser, P., Frétigny, C. and Desbarres, J., *Sructure Fine d'Absorption X en Chimie*. Ecole du C.N.R.S, Garchy, 1988 p. 1.
30. Loudjani, M. K., Cortès, R., Roy, J. and Huntz, A. M., Study by extended X-ray absorption fine-structure technique and microscopy of the chemical state of yttrium in α-polycristalline alumina. *J. Am. Ceram. Soc*., 1985, **68**(11), 559–562.
31. Loudjani, M. K. and Cortès, R., X-ray absorption study of the local structure and the chemical state of yttrium in polycristalline α-alumina. *J. Eur. Ceram. Soc*., 1994, **14**, 67–75.
32. Garvie, R. C., The occurrence of metastable tetragonal zirconia as a crystalline size Effect. *J. Phys. Chem*., 1965, **69**, 1238–1243.
33. Yuren, W., Kunqan, L., Dazhi, W., Zhonghua, W. and Zhengzhi, F., The EXAFS study of nanocrystalline zirconia. *J. Phys. Condens. Matter*, 1994, **6**, 633–640.
34. Robin, W., Grimes: solution of MgO, CaO, and TiO_2 in α-Al_2O_3. *J. Am. Ceram. Soc*., 1994, **77**(2), 378–384.
35. Peter, K., Lagerlöf, D., Heuer, A. H., Castaing, J., Rivière, J. P. and Mitchell, T. E., Slip and twinning in saphire (α-Al_2O_3). *J. Am. Ceram. Soc*., 1994, **77**(2), 385–397.